C3a/C3aR axis is involved in diabetic kidney injury by regulating podocyte mitophagy in diabetic nephropathy

MENGJIE WENG[1-3*], XIAOTING WU[1-3*], SIYI RAO[1-3*], KUN NIE[1-3], DANYU YOU[1-3], TINGTING ZHENG[1-3], ENQIN LIN[1-3], JING ZHENG[1-3], JIONG CUI[1-3] and JIANXIN WAN[1-3]

[1]Department of Nephrology, Blood Purification Research Center, The First Affiliated Hospital, Fujian Medical University, Fuzhou, Fujian 350005, P.R. China; [2]Fujian Clinical Research Center for Metabolic Chronic Kidney Disease, The First Affiliated Hospital, Fujian Medical University, Fuzhou, Fujian 350005, P.R. China; [3]Department of Nephrology, National Regional Medical Center, Binhai Campus of The First Affiliated Hospital, Fujian Medical University, Fuzhou, Fujian 350207, P.R. China

Received June 20, 2025; Accepted October 2, 2025

DOI: 10.3892/ijmm.2025.5664

Abstract. The C3a/C3aR axis has been confirmed to be associated with the pathogenesis of diabetic nephropathy (DN) and mitochondrial dysfunction; however, the exact mechanisms underlying its role in diabetic podocytopathy remain unclear. The present study investigated the involvement of C3a/C3aR signaling in regulating mitophagy during the progression of DN. Diabetic db/db mice exhibited elevated renal C3 and C3aR levels, concurrent with podocyte injury, proteinuria and glomerular damage. Administration of the C3aR antagonist (C3aRA) SB290157 attenuated podocyte loss, reduced albuminuria and mitigated glomerular pathology. Ultrastructural and functional analyses revealed that C3aRA restored mitochondrial integrity in podocytes, resolving diabetes-associated fragmentation and bioenergetic deficits. In vitro, high glucose-exposed human podocytes displayed suppressed mitophagy and mitochondrial dysfunction, which were exacerbated by exogenous C3a. Conversely, C3aRA treatment enhanced mitophagy and preserved mitochondrial membrane potential, while small interfering RNA-mediated C3aR or PINK1 knockdown abolished these protective effects. Notably, C3aRA activated the PI3K/AKT/FoxO1 pathway, driving both mitochondrial biogenesis and mitophagy. Disruption of this axis via FoxO1 inhibition reversed the therapeutic benefits of C3aRA, confirming its mechanistic centrality. In conclusion, the C3a/C3aR/PI3K/AKT/FoxO1 axis represents a previously unrecognized molecular bridge between complement activation and mitophagy failure in DN. Pharmacological disruption of this pathway could preserve podocyte homeostasis, offering a precision strategy against diabetic kidney injury.

Correspondence to: Professor Jianxin Wan or Professor Jiong Cui, Department of Nephrology, Blood Purification Research Center, The First Affiliated Hospital, Fujian Medical University, 20 Chazhong Road, Taijiang, Fuzhou, Fujian 350005, P.R. China
E-mail: wanjx@fjmu.edu.cn
E-mail: xiaoqingcj@aliyun.com

*Contributed equally

Key words: C3a/C3aR axis, diabetic nephropathy, mitophagy, *PI3K/AKT/FoxO1* signaling, podocyte injury

Introduction

Diabetic nephropathy (DN), one of the most devastating microvascular complications of diabetes mellitus, manifests initially as microalbuminuria and progressively evolves into end-stage renal disease through characteristic glomerulopathic changes (1). This trajectory underscores the critical need to elucidate its molecular pathogenesis and develop targeted interventions for early renal preservation. Previous evidence implicates glomerular podocytes as primary targets in diabetic renal injury, where their structural and functional integrity governs glomerular filtration barrier competence (2). Notably, the high mitochondrial density in these specialized epithelial cells, which rely predominantly on oxidative phosphorylation for energy homeostasis, renders them particularly vulnerable to metabolic disturbances. Consequently, podocyte mitochondrial dysfunction is increasingly recognized as a pivotal driver of DN progression, involving disrupted energy metabolism, exacerbated oxidative stress, and impaired organelle quality control mechanisms (3).

Emerging evidence indicates that complement system activation, particularly through the C3a/C3aR axis, is involved in progressive DN (4,5). Substantial studies demonstrate that C3aR blockade reduces podocyte mitochondrial dysfunction and oxidative stress while alleviating renal damage in DN rodent models (6-8). Mitophagy, a selective autophagic process essential for cellular homeostasis, eliminates damaged mitochondria via lysosomal degradation (9). In early diabetes, renal cells exhibit enhanced clearance of glucose-damaged mitochondria. However, disease progression coincides with increased mitochondrial fission, heightened oxidative stress and defective mitophagy. This failure to eliminate compromised mitochondria permits damaging factor release (reactive oxygen species), thus driving DN advancement (10). In both high-glucose environments and DN models, a decrease in the expression of key proteins involved in mitophagy, such as

PINK1, parkin and microtubule-associated protein 1A/1B-light chain 3B (LC3B), has been observed in podocytes. Conversely, the expression of P62, an indicator of impaired autophagy, significantly increases (11-13). These findings suggest that dysfunction in podocyte mitophagy may play a crucial role in the pathogenesis of DN.

Despite evidence linking C3a/C3aR to DN, the mechanisms underlying its role in podocyte mitophagy remain unclear. While our prior clinical and animal data demonstrated local complement C3 activation and reduced mitophagy in DN, the direct regulatory involvement of C3a/C3aR in mitophagy downregulation remains undefined. The current study aimed to evaluate C3a/C3aR effects on glomerular podocytes utilizing both human podocyte cultures and db/db murine models. Markedly increased renal C3 and C3aR expression was observed in diabetic mice and high glucose (HG)-exposed podocytes. Importantly, a novel regulatory role for C3a/C3aR was identify in maintaining podocyte mitochondrial homeostasis through PI3K/AKT/FoxO1 signaling-mediated mitochondrial biogenesis and mitophagy. These findings suggest that targeting C3aR to preserve mitochondrial function and cellular bioenergetics upstream of cellular damage represents a promising therapeutic strategy for DN.

Materials and methods

Gene expression profiling data and preprocessing. Transcriptomic profiles of human kidney podocytes were retrieved from the Gene Expression Omnibus (accession no. GSE47183), comprising 122 samples across eight pathological categories, including DN (n=14), focal segmental glomerulosclerosis (FSGS, n=23), FSGS with minimal change disease (MCD, n=6), membranous glomerulonephritis (n=21), MCD (n=15), rapidly progressive glomerulonephritis (RPGN, n=23), thin membrane disease (TMD, n=3), and tumor nephrectomy controls (n=17) (14,15), The dataset was normalized using Robust Multichip Average standardization with the affy package (v1.78.0; Bioconductor Release 3.18, https://bioconductor.org). After normalization, the platform file was used to map each probe to Entrenz Gene ID. If a probe maps to multiple genes or does not map to any genes, the expression value of the probe is deleted. If multiple probes map to the same gene, the average value of these probes is taken as the expression value of the gene. The normalized data was visualized using pheatmap (Bioconductor pheatmap package).

Animals and reagents. Male C57BLKS/JGpt wild-type (wt/wt, 8-week-old, 20-25 g, n=10) and db/db mice (8-week-old, 45-55 g, n=20) were procured from GemPharmatech Co., Ltd. All procedures were conducted in accordance with the NIH Guide for the Care and Use of Laboratory Animals (16) and approved by the Institutional Animal Care and Use Committee of Fujian Medical University (approval no. IACUC FJMU 2023-Y-1033; Fuzhou, China). Animals were maintained under standardized conditions (12/12-h light/dark cycle, 22±2˚C, 60% humidity) with ad libitum access to food and water. Following a 7-day acclimatization period, wt/wt mice served as non-diabetic controls (NC, n=6). Diabetic db/db mice were randomly allocated into two experimental groups (n=6/group): i) A C3aR antagonist (C3aRA)-treated group, which received intraperitoneal injections of SB290157 (10 mg/kg; cat. no. HY-101502A/CS-6852; MedChemExpress) every 48 h (17); and ii) a vehicle group, which received equivalent volumes of 5% DMSO in sterile saline. SB290157 was freshly reconstituted in vehicle solution (5% DMSO in 0.9% NaCl) under aseptic conditions. All solutions were filtered through 0.22-μm membranes prior to administration. After 8 weeks of intervention, 24-h urine was collected from all mice using a metabolic cage (Fig. S1). Euthanasia was performed by intraperitoneal injection of 2% sodium pentobarbital at a dose of 100 mg/kg. Next, bilateral kidneys were excised, the renal capsule was removed, and the kidneys were sectioned by sagittal. Kidney tissue was either fixed with 4% paraformaldehyde at 4˚C for 24 h or rapidly frozen in liquid nitrogen.

Measurement of serum creatinine, urinary albumin/creatinine ratio (UACR), 24-h urinary total protein (UTP) and cell-culture medium C3a level. Metabolic cages were used to collect 24h urine samples. The contents of serum creatinine, 24-h UTP and UACR were measured using an automatic biochemical analyzer (Beckman Coulter, Inc.). Cell-culture medium C3a levels were measured by using ELISA kits (Human Complement C3a; cat. no. USEA387Hu; Wuhan Cloud-Clone Corp.), according to the manufacturer's protocol.

Histological analysis. Kidney sections were deparaffinized and rehydrated and were then stained with hematoxylin and eosin (H&E), and Periodic Acid-Schiff (PAS).

Cell culture. An immortalized human podocyte cell line was donated by Professor Moin A. Saleem (Bristol University, UK) and was retained and donated by the Nephrology Laboratory of Wuhan University. Cells were cultured in low-glucose Roswell Park Memorial Institute (RPMI)-1640 medium (Gibco; Thermo Fisher Scientific, Inc.) with 10% fetal bovine serum (FBS; Gibco; Thermo Fisher Scientific, Inc.). The human immortalized podocytes used in the present study were of passages 16-23. The podocytes were propagated at 33˚C and treated with interferon [insulin-Transferrin-Selenium (ITS)-G; 10 U/ml; Invitrogen; Thermo Fisher Scientific, Inc.]. Next, cells were differentiated without ITS-G at 37˚C for 7 days. For further evaluation, the podocytes were stimulated with HG (30 mM glucose) and mannitol (24.5 mM mannitol+5.5 mM glucose) containing 1% FBS with or without incubation with C3a or C3aRA (SB290157) for 24 h.

Application of small interfering RNA (siRNA). A duplex siRNA was designed to target human C3aR (NCBI: NM 004054.4; https://www.ncbi.nlm.nih.gov/nuccore/?term=NM+004054.4). The target sequence is GCUUCAAAC AACCUCUAAU (1746-1764 bp) and the siRNA nucleotide sequences for C3aR were r(GCCUCAAACAACCUCUAAU) dTdT (Sense) and r(AUUAGAGGUUGUUUGAGGC) dGdG (Antisense). A duplex siRNA was designed to target human PINK1 (NCBI: NM 032409.3; https://www.ncbi.nlm.nih.gov/nuccore/?term=NM+032409.3). The target sequence is GCTGGAGGAGTATCTGATA (1,449-1,467 bp) and the siRNA nucleotide sequences for PINK1 were r(GCUGGA GGAGUAUCUGAUA) dTdT (Sense) and r(UAUCAGAUA CUCCUCCAGC) dGdG (Antisense). Meanwhile, Negative

control (NC) siRNA with no homology to mammalian genomes served as negative control, which nucleotide sequences were r (UUCUCCGAACGUGUCACGU) dTdT (Sense) and r (ACG UGACACGUUCGGAGAA) dTdT (Antisense). All siRNAs were synthesized by Shanghai Hanheng Biotechnology Co., Ltd. For transfection, cells were seeded at 60% confluency in antibiotic-free medium and transfected with 50 nM siRNA using RNAFit™ Transfection Reagent (cat. no. HB-RF-1000; Shanghai Hanheng Biotechnology Co., Ltd.). Cells were harvested 48 h post-transfection for downstream analysis, with protein expression verification performed by western blotting (Fig. S2).

TdT-mediated dUTP nick-end labeling (TUNEL) assay. Paraffin-embedded kidney sections and cell slides were processed with a TUNEL assay kit (Dalian Meilun Biology Technology Co., Ltd.) to detect apoptosis. Paraffin-embedded renal sections were deparaffinized using xylene and rehydrated with ethanol. Cells were fixed with 4% paraformaldehyde at 37˚C for 10 min. The deparaffinized sections and fixed cell slides were incubated first with 20 μg/ml DNase-free proteinase K for 30 min at room temperature and then with TdT reaction mix for 60 min at 37˚C in the dark. Next, nuclei were counterstained with DAPI (0.001 mg/ml). Images were acquired with a fluorescence microscope. The apoptotic cells were identified and quantified by counting the number of positive cells in three fields per group.

Immunohistochemistry. Xylene and ethanol were used to deparaffinize and dehydrate renal sections, respectively, and citrate buffer was used for antigen retrieval. The sections were incubated with antibodies against C3 (1:5,000; Santa Cruz Biotechnology, Inc.), C3aR (1:5,000; Santa Cruz Biotechnology, Inc.), Mnf2 (1:1,000; Proteintech Group, Inc.) or PINK1 (1:1,000; Proteintech Group, Inc.) at room temperature for 1 h. Next, the sections were stained with an enhanced polymer detection system (Beijing Zhongshan Jinqiao Biotechnology Co., Ltd.) according to the manufacturer's instructions. Diaminobenzidine was used as an HRP-specific substrate.

Immunofluorescence. Renal tissue sections and cell slides were washed with PBS, permeabilized with PBS containing 0.3% Triton X-100 and blocked with 5% BSA (Gibco; Thermo Fisher Scientific, Inc.) at 37˚C for 30 min. Next, samples were incubated with a primary antibody overnight at 4˚C. The following antibodies were employed: Mouse anti-TOMM20 (1:100; cat. no. 11802-1-AP; Proteintech Group, Inc.), rabbit anti-synaptopodin (1:200; cat. no. ab224491; Abcam) and guinea pig anti-nephrin (1:200; cat. no. GP-N2; ProGen). After PBS washing, sections were incubated for 1 h at room temperature with goat anti-guinea pig, goat anti-mouse, or goat anti-rabbit secondary antibodies conjugated with Alexa Fluor™ 488 or 594, followed by treatment with DAPI (0.001 mg/ml) for 10 min at room temperature. Quantification of the TOMM20/nephrin toward staining was performed in 10-15 glomeruli per section using ImageJ 1.40g (National Institutes of Health), and data were expressed as a percentage of the TOMM20/nephrin co-staining area (yellow) on the total glomerular TOMM20 area (red). Samples were examined under a confocal inverted laser microscope (LSM 510 Meta; Carl Zeiss AG).

Preparation of C3a solution. Human complement C3a (cat. no. 204881; 50 μg; Merck KGaA) was diluted to a concentration of 5-10 M using sterile PBS at a pH of 7.2. The resulting solution was aliquoted into 50 μl portions and stored at -80˚C. This solution was utilized for extrinsic interventions on podocytes at different time points and concentrations.

Cytoskeleton visualization. Cells were fixed with 4% paraformaldehyde at 37˚C for 15 min, permeabilized with PBS containing 0.3% Triton X-100, blocked with 5% BSA for 30 min and stained with 500 nM Alexa Fluor™ 488 phalloidin (Invitrogen; Thermo Fisher Scientific, Inc.) for 30 min and DAPI (0.001 mg/ml) for 15 min. The cytoskeleton was visualized in the composite image of the F-actin (phalloidin, green). The average intensity of F-actin was measured using ImageJ 1.40g software.

Double labeling GFP/LC3B-DsRed/Mito adenovirus mitophagy assay. A mixture of 20 μl DsRed-Mito (red) adenovirus stock solution ($1x10^{10}$ PFU/ml) + 20 μl GFP-LC3B (green) adenovirus stock solution ($1x10^{10}$ PFU/ml) + 160 μl RPMI-1640 medium was prepared to make a final volume of 200 μl adenovirus mix ($1x10^{9}$ PFU/ml). Podocytes were washed with PBS three times for 3 min each, and 250 μl RPMI-1640 medium was added to each well. Next, 15 μl of the adenovirus mix (optimal MOI=100, Fig. S3) was added to each well, and after 4 h of infection, an additional 250 μl RPMI-1640 medium was added. Next, the virus-containing medium was aspirated, and complete medium was added for 12-h incubation. Subsequently, cells were fixed, their nuclei were stained, and images were captured. By utilizing the dual fluorescence adenovirus system (GFP/LC3B-DsRed/Mito), the dynamic process of mitophagy could be precisely tracked in real-time tracked. Quantification of *GFP-LC3B* (green)-associated Mito-DsRed (red) staining was performed using ImageJ 1.40g software. Analysis included determining the total number of LC3-positive points and the percentage of Mito-LC3B overlap among LC3-positive points. Each experiment involved analyzing at least ≥5 cells.

Western blotting. Proteins were extracted from kidney tissues and podocytes using RIPA lysis buffer (cat. no. P0013B; Beyotime Institute of Biotechnology) containing a protease inhibitor cocktail (cat. no. P1005; Beyotime Institute of Biotechnology) and a phosphatase inhibitor cocktail (cat. no. P1082; Beyotime Institute of Biotechnology). Tissue homogenates were centrifuged at 12,000 x g for 15 min at 4˚C, the protein concentrations of supernatants were determined by using a BCA protein assay kit (cat. no. P0009; Beyotime Institute of Biotechnology) and stored at -80˚C. Equal amounts of proteins (40 μg) were loaded per lane on a 10% SDS-PAGE gel and transferred to polyvinylidene difluoride (PVDF) membranes (MilliporeSigma), which were blocked with 5% non-fat milk for 2 h at room temperature. Next, the membranes were incubated with primary antibody against βactin (1:2,000; cat. no. A1978; MilliporeSigma), C3 (1:500; cat. no. sc-28294; Santa Cruz Biotechnology, Inc.), C3aR

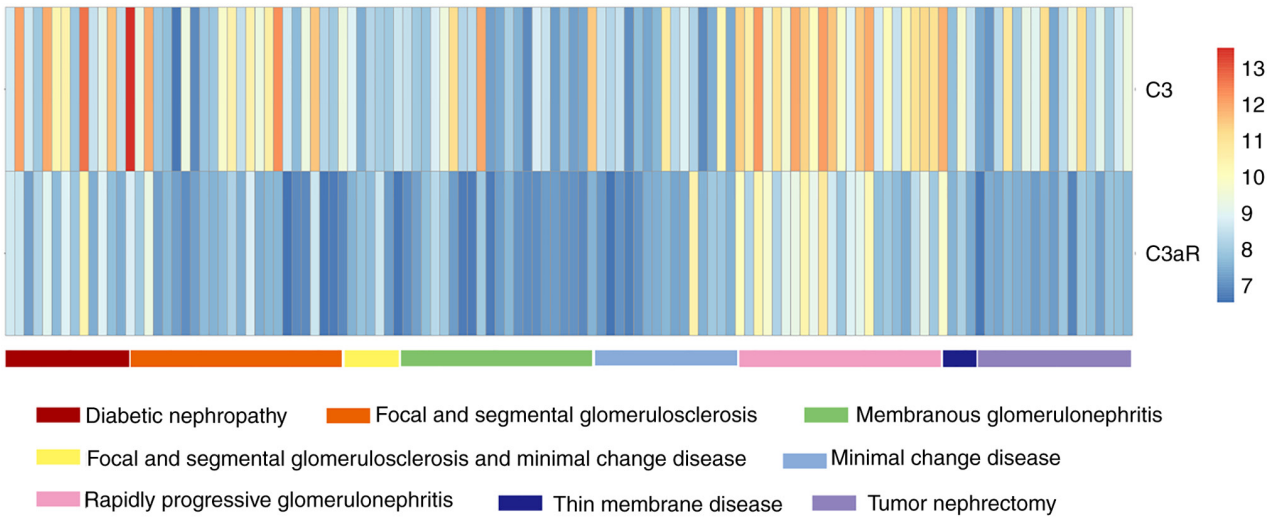

Figure 1. Heatmap of the *C3* and *C3aR* transcriptome data in different kidney-related diseases. A set of kidney disease-related transcriptome data was collected from the Gene Expression Omnibus database using Affymetrix microarray sequencing technology. This dataset (GSE47183) contained 122 human renal podocyte samples (including 14 samples of diabetic nephropathy, 23 samples of focal and segmental glomerulosclerosis, 6 samples of focal and segmental glomerulosclerosis and MCD, 21 samples of membranous glomerulonephritis, 15 samples of MCD, 23 samples of rapidly progressive glomerulonephritis, 3 samples of thin membrane disease and 17 samples of tumor nephrectomy). Red indicates high expression, while blue indicates low expression. MCD, minimal change disease.

(1:500; cat. no. sc-53738; Santa Cruz Biotechnology, Inc.), parkin (1:1,000; cat. no. 14060-1-AP; Proteintech Group, Inc.), PINK1 (1:500; cat. no. 23274-1-AP; Proteintech Group, Inc.), TOMM20 (1:500; cat. no. 11802-1-AP; Proteintech Group, Inc.), LC3B (1:1,000; cat. no. ab192890; Abcam), ZO1 (1:1,000; cat. no. ab96587; Abcam), synaptopodin (1:1,000; cat. no. ab224491; Abcam), podocin (1:1,000; cat. no. ab50339; Abcam), PI3K [p85α (54 + 85 kDa); 1:1,000; cat. no. MA5-14942; Invitrogen; Thermo Fisher Scientific, Inc.), phosphorylated (p)-A*KT* (1:1,000; cat. no. MA5-14952; Invitrogen; Thermo Fisher Scientific, Inc.) and FoxO1 (1:1,000; cat. no. MA5-17151; Invitrogen; Thermo Fisher Scientific, Inc.) at 4˚C overnight. Blots were incubated with Goat anti-Rabbit IgG (H+L) HRP conjugate (cat. no. ab6721; Abcam) or Goat anti-mouse IgG (H+L) HRP conjugate (cat. no. ab6789; Abcam) at 1:10,000 dilution in 5% non-fat milk/TBST for 1 h at 25˚C. Images were analyzed in ImageJ (v1.54f; National Institutes of Health) using the Gel Analyzer tool. Rolling ball radius (50 pixels) was applied for background subtraction.

Transmission electron microscopy (TEM). Mouse kidneys were fixed in 2.5% glutaraldehyde and 0.05 M sodium phosphate buffer (Ph 7.2) overnight at 4˚C. Samples were embedded in epoxy resin after being washed with 0.1 M cacodylate buffer and saline, followed by a gradual series of ethanol dehydration. Sections (60-90 nm thickness) were then incubated on copper grids, contrasted with aqueous uranyl acetate and lead citrate, and analyzed. Images were recorded with a TEM (H7500; Hitachi, Ltd.).

Statistical analysis. All data are expressed as the mean ± standard error of the mean. Comparisons between two groups were performed using a paired Student's ttest. For multiple groups, the data were analyzed by one- or twoway ANOVA, followed by Bonferroni post hoc tests, where appropriate. $P<0.05$ was considered to indicate a statistically significant difference. All statistical analyses were performed using GraphPad Prism 8.3.0 software (GraphPad; Dotmatics).

Results

Expression of C3 and C3aR in different kidney-related diseases. The results of the present study were analyzed by comparing the expression levels of the same gene in different kidney-related diseases. As shown in Fig. 1, the expression levels of C3 and C3aR were relatively high in RPGN and DN, compared with the other kidney-related diseases, indicating that the activation of complement *C3* may be closely related to the occurrence and development of DN.

Inhibiting C3aR shows promise in ameliorating renal damage in DN mice. Further validation was conducted *in vivo* in a DN model (db/db mice). Although serum C3a levels showed no significant difference (Fig. S4), renal C3 and C3aR protein expression was significantly increased in DN mice versus non-diabetic controls (Fig. 2A). Glomerular-localized *C3*/*C3a*R proteins levels (Fig. 2B) were substantially reduced following SB290157 treatment. Histological analysis revealed that db/db mice exhibited glomerular hypertrophy, mesangial hyperplasia, increased cellularity and matrix expansion (H&E and PAS staining; Fig. 2C). C3aRA intervention attenuated mesangial matrix deposition without exacerbating cellular proliferation. Biochemical assessments demonstrated significantly elevated UACR, 24 h-UTP, blood glucose levels, total cholesterol, or triglyceride levels and kidney/body weight ratios (Table SI) in db/db mice versus controls, despite non-significant differences in serum creatinine. Electron microscopy confirmed diffuse podocyte foot process effacement with increased renal apoptosis. C3aRA treatment significantly reduced body weight (Fig. S5), UACR and 24 h-UTP, restored organized foot process architecture, and diminished apoptosis (Fig. 2D-F). Collectively, these data indicated that *C3aR*

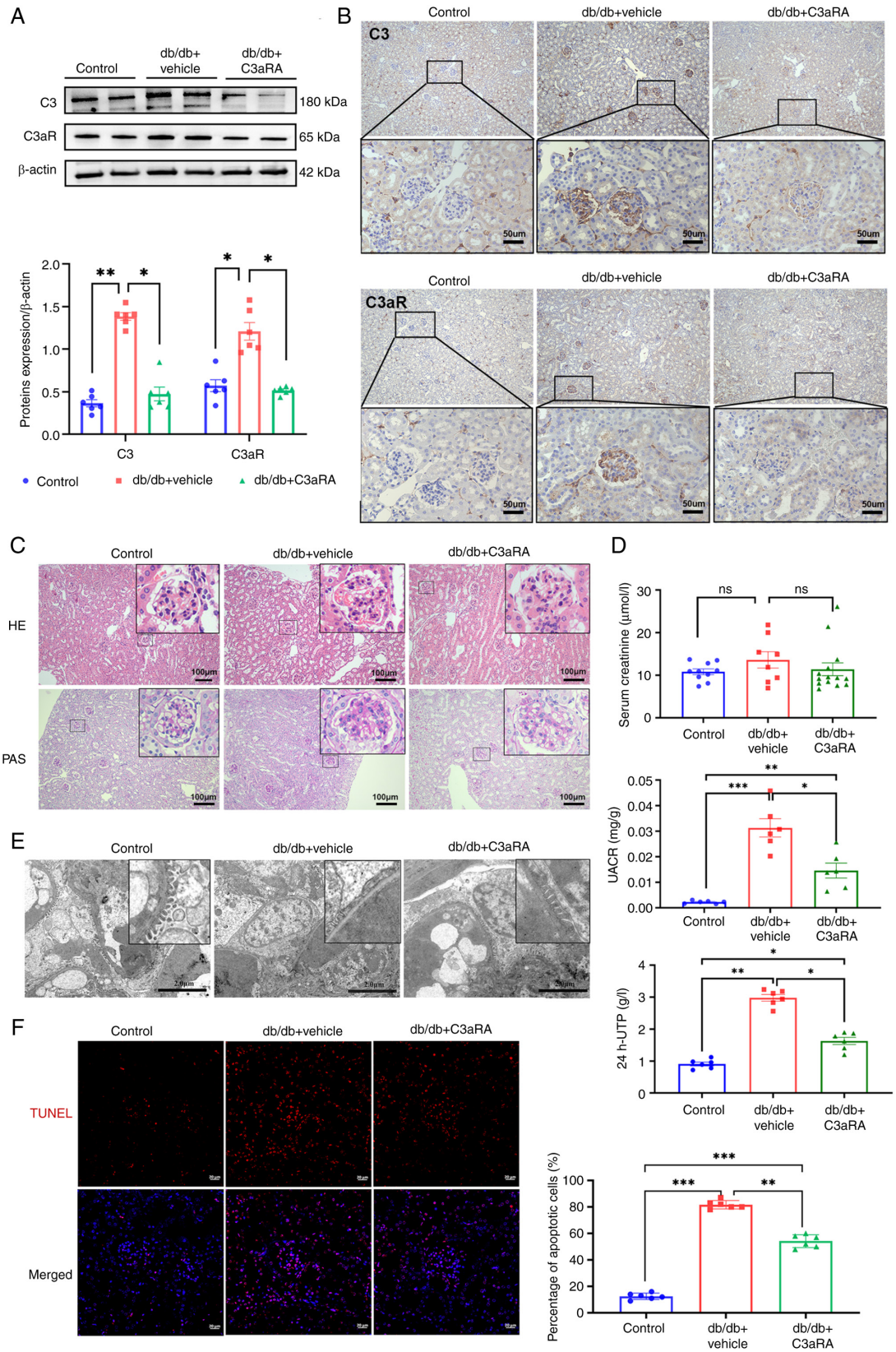

Figure 2. Expression of complement *C3*, *C3aR* and renal injury in each mouse group. (A) Protein levels of *C3* and *C3aR* in kidney tissues (n=6). Corresponding histograms of the representative protein bands are shown on the bottom panel. (B) Immunohistochemical detection of the deposition and expression of complement *C3* and *C3aR* in kidney tissue specimens of each mouse group. Microscopic images are shown at x100 and x400 magnification. (C) Hematoxylin and eosin, and Periodic Acid-Schiff staining of kidney tissues in each group of mice. Microscopic images are shown at x100 magnification. (D) Levels of blood creatinine, 24 h-urinary total protein and urine albumin/creatinine ratio in each group of mice (n=6). (E) Transmission electron microscopy observation of the ultrastructure of glomerular podocytes. Scale bar, 2.0 μm. (F) TdT-mediated dUTP nick-end labeling assay detection of apoptotic cells in mouse kidney tissues for each group. Immunofluorescence images are shown, and statistical analysis of the percentage of apoptotic cells for each group is shown on the right side of the representative image (n=6). Scale bar, 20 μm. *db/db* mice were used to establish a diabetic nephropathy model. SB290157 is a *C3aR* antagonist. Data are expressed as the mean ± SEM and analyzed by two-way ANOVA with Bonferroni correction. *P<0.05, **P<0.01 and ***P<0.001. C3aRA, C3aR antagonist; ns, no statistically significant difference.

antagonism ameliorates proteinuria and histopathological damage in experimental DN.

C3aR inhibition ameliorates podocyte dysfunction and mitochondrial injury in diabetic mice. Accumulating evidence has identified podocyte injury as a critical pathogenic mechanism in DN progression (11,18). Immunofluorescence analysis demonstrated significantly diminished fluorescence intensity and disrupted cytoskeletal architecture in db/db podocytes. C3aRA intervention upregulated synaptopodin and nephrin expression in DN models (Fig. 3A). Protein quantification revealed marked downregulation of the glomerular filtration barrier components ZO-1 and podocin in db/db renal tissues versus controls, and these effects were reversed by C3aR blockade (Fig. 3B).

The mitochondrial integrity regulators Mfn2 (fusion protein) and TOMM20 (a translocase of the outer mitochondrial membrane) exhibited significantly reduced glomerular deposition in db/db mice (Fig. 3C and D). Ultrastructural analysis confirmed mitochondrial swelling, matrix disorganization and cristae fragmentation (Fig. 3E). C3aRA treatment normalized Mfn2 and TOMM20 expression (Fig. 3C and D) and restored mitochondrial morphology (Fig. 3E), indicating significant attenuation of podocyte mitochondrial damage.

Comparative analysis of mitophagy and signaling pathway alterations in DN. Western blot analysis of renal tissue homogenates revealed significantly reduced expression of the mitophagy markers LC3B-II/LC3B-I, PINK1 and parkin in DN model mice versus controls (Fig. 4B). Immunohistochemistry demonstrated diminished PINK1 deposition in both glomerular and tubular compartments of db/db mice, with pronounced reduction in glomeruli (Fig. 4A). Notably, intraperitoneal administration of SB290157 partially reversed these alterations, significantly elevating LC3B-II/LC3B-I, PINK1 and parkin protein levels (Fig. 4B) while enhancing glomerular PINK1 deposition (Fig. 4A). These findings indicated that C3aRA mitigates impaired autophagic flux and enhances PINK1-mediated mitophagy in diabetic kidneys.

It was observed in previous experiments by the authors that p-AKT was activated in renal tissues of db/db mice, while t-AKT expression levels remained stable (Fig. S6A). Further immunoblotting demonstrated PI3K/AKT pathway activation in diabetic renal tissue, characterized by increased PI3K expression and p-AKT, concomitant with FoxO1 suppression (Fig. 4C). C3aR antagonism significantly attenuated PI3K/p-AKT upregulation while restoring FoxO1 expression (Fig. 4C), indicating that modulation of this signaling axis contributes to the therapeutic effect.

HG and C3a induce podocyte injury and suppress mitophagy in vitro. The C3/C3aR axis is implicated in impaired podocyte mitophagy in DN. To investigate this mechanistically, hyperglycemic injury was modeled *in vitro* by using conditionally immortalized podocytes. Podocytes were cultured for 24 h under normal glucose (NG, 5.5 mM glucose), HG (30 mM glucose) or mannitol high osmotic control (MG, 24.5 mM mannitol + 5.5 mM glucose) conditions. HG-exposed podocytes exhibited F-actin disassembly with reduced fluorescence intensity versus NG/MG controls (Fig. 5A), which was accompanied by significant downregulation of synaptopodin and podocin (Fig. 5B). C3aR expression significantly increased under HG conditions (Fig. 5D). ELISA revealed time-dependent C3a accumulation in supernatants, with HG cultures showing accelerated generation (≤96 h) despite comparable cellular C3 expression across groups (Fig. 5C). Mitophagy markers (LC3B-II/LC3B-I, PINK1 and parkin) were significantly suppressed in HG-treated podocytes (Fig. 5E), confirming complement axis activation and mitophagy impairment.

Complementing these findings, direct C3a exposure (10^{-7} M) induced dose- and time-dependent cytoskeletal disorganization, which was most pronounced at 24 h (Fig. 5G). Concomitant reductions in PINK1 and parkin expression demonstrated C3a's causal role in mitophagy suppression (Fig. 5F), establishing its direct contribution to podocyte injury.

C3aR knockdown ameliorates HG-induced podocyte injury and mitophagy suppression. To mechanistically validate the involvement of the C3a/C3aR axis in podocyte injury and mitophagy impairment under hyperglycemic conditions, siRNA-mediated C3aR downregulation was employed in cultured podocytes. Comparative analysis revealed that both HG-exposed and HG + NC siRNA groups exhibited fragmented F-actin microfilaments with cytoskeletal disorganization, elevated apoptotic indices, mitochondrial swelling with cristae fragmentation, and minimal autolysosome formation, which collectively indicate profound mitochondrial damage and suppressed autophagic flux (Fig. 6A-C). By contrast, C3aR-knockdown podocytes under HG conditions demonstrated restored F-actin bundling with increased filament density, reduced apoptosis, preserved mitochondrial ultrastructure (characterized by mild swelling and intact cristae), decreased proportions of damaged mitochondria and a significant increase in autophagosome-engulfed mitochondria.

For dynamic quantification of mitophagic flux, adenoviral transduction of GFP-LC3B/DsRed-Mito reporters revealed significantly fewer mitochondrial $LC3^+$ puncta in the HG and HG + NC siRNA groups versus normoglycemic controls ($P<0.01$), indicative of impaired mitophagosome biogenesis. This deficit was reversed by C3aR knockdown, which increased mitochondrial $LC3^+$ puncta by 2.1-fold (Fig. 6D). Immunoblot analysis further confirmed that C3aR silencing significantly upregulated the LC3B-II/LC3B-I ratio (1.8-fold, $P<0.001$), as well as PINK1 (1.5-fold, $P<0.01$), and parkin (1.7-fold, $P<0.001$) expression levels in HG-treated podocytes (Fig. 6E), establishing that C3aR blockade restores mitophagic activity in DN.

C3a/C3aR axis suppresses mitophagy via PI3K/AKT/FoxO1 signaling in hyperglycemia-induced podocyte injury. To delineate the role of C3a/C3aR in diabetic podocyte dysfunction, PINK1 knockdown was combined with C3aRA. HG-exposed podocytes exhibited cytoskeletal disorganization and elevated apoptosis, and these phenotypes partially ameliorated by C3aRA. Crucially, PINK1-silenced podocytes (HG + C3aRA + PINK1 siRNA) displayed exacerbated F-actin fragmentation with reduced fluorescence intensity and increased apoptosis compared with HG + C3aRA and HG + C3aRA + NC siRNA controls (Fig. 7A). Immunoblot analysis confirmed that

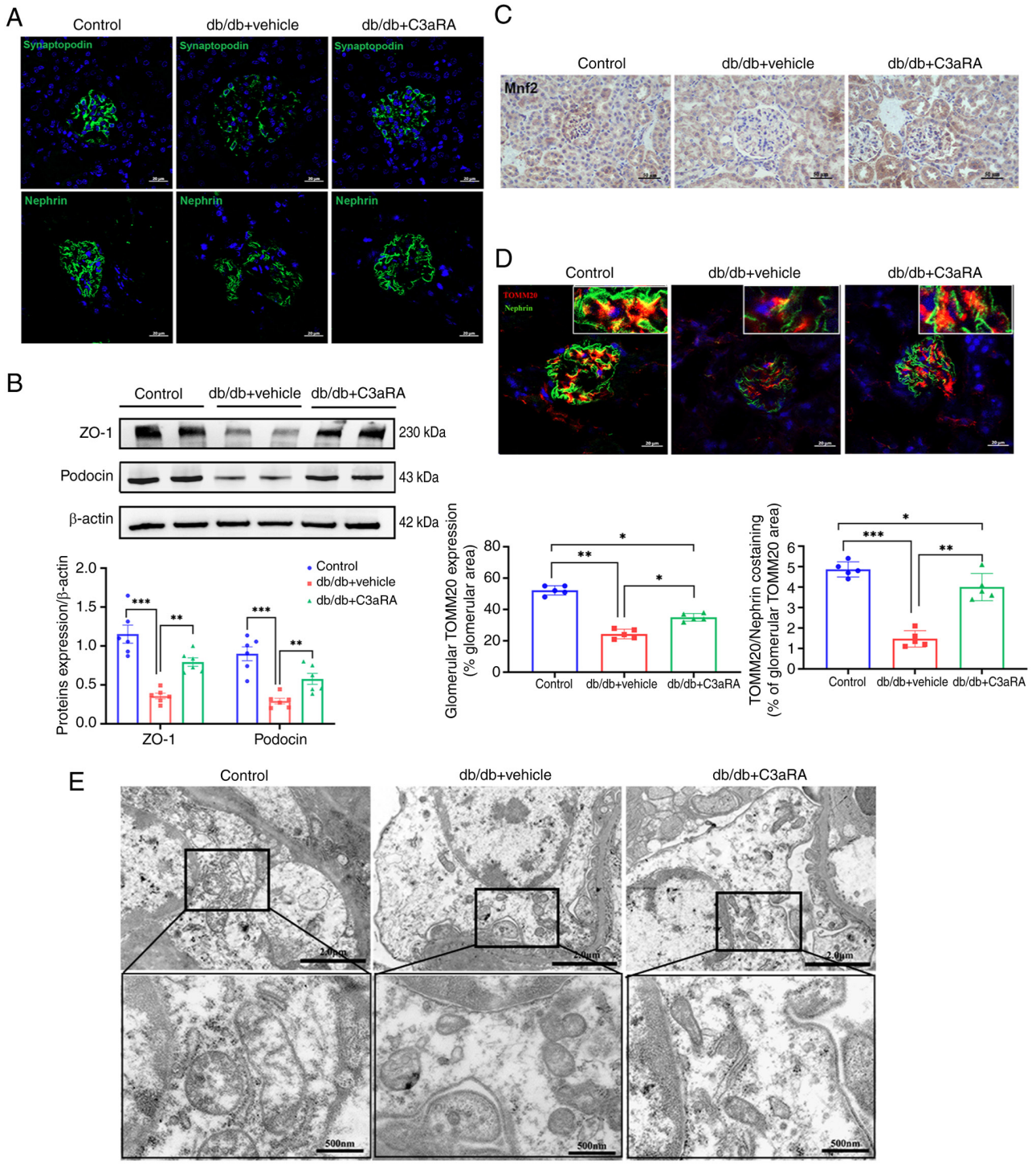

Figure 3. Function of glomerular podocytes and mitochondrial damage in each group of mice. (A) Immunofluorescence images of the podocyte-specific functional proteins *synaptopodin* and *nephrin* in each group of mice. Scale bar, 20 μm. (B) Protein levels of *ZO-1* and podocin in the kidney tissues (n=6). Corresponding histograms are shown on the bottom panel of representative protein bands. (C) Immunohistochemical analysis of the mitochondrial fusion protein *Mnf2*. Scale bar, 50 μm. (D) Representative images and quantification of double immunofluorescence staining for *TOMM20* (red) and *nephrin* (green) in the glomerulus of mice. The yellow areas indicate *TOMM20* and *nephrin* colocalization in podocytes (n=6). Scale bar, 20 μm. (E) Electron microscopy image of mitochondrial morphology in podocytes. Scale bar, 2.0 μm and 500 nm. Data are expressed as the mean ± SEM and analyzed by two-way ANOVA with Bonferroni correction. *P<0.05, **P<0.01 and ***P<0.001. C3aRA, C3aR antagonist.

PINK1 knockdown significantly reduced mitophagy markers (PINK1, parkin and LC3B-II/LC3B-I ratio) and diminished the levels of key podocyte integrity proteins (ZO-1, synaptopodin and podocin) and of the mitochondrial translocase TOMM20 (P<0.05). Importantly, PINK1 silencing attenuated C3aRA-mediated protection against HG-induced injury, indicating that C3a/C3aR induces podocyte damage through PINK1-mediated mitophagy impairment (Fig. 7B). Following pretreatment of podocytes with HG and HG + C3a, activation of p-AKT was observed (Fig. S6B). Mechanistically, C3a stimulation significantly enhanced PI3K/AKT phosphorylation while suppressing FoxO1 expression versus normoglycemic

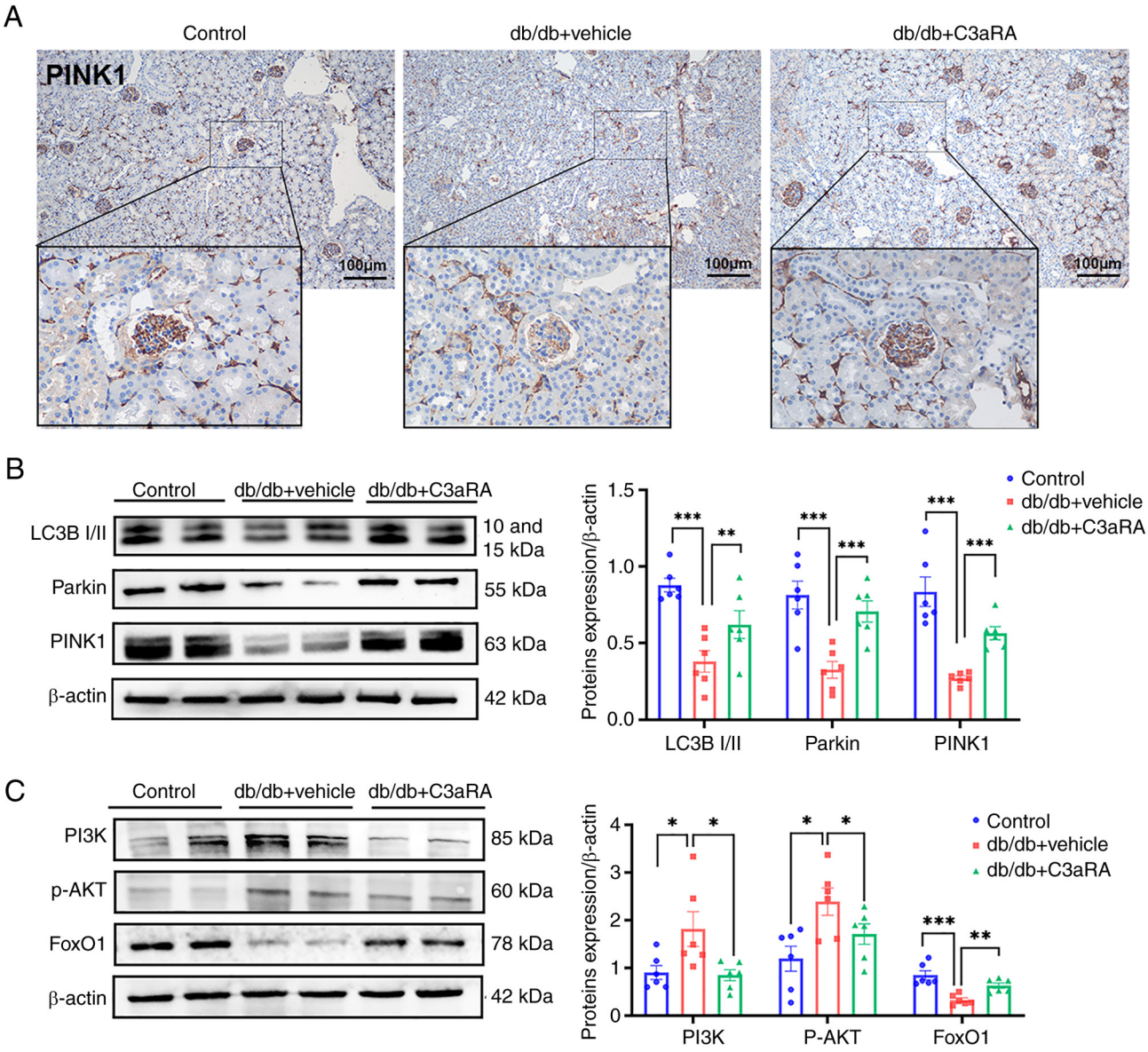

Figure 4. Expression levels of mitophagy and related pathway proteins in mouse renal tissues. (A) Immunohistochemical analysis of the mitophagy-specific protein PINK1. Magnification, x100. (B) Protein levels of LC3B I/II, parkin and PINK1 in kidney tissues (n=6). Corresponding histograms are shown on the right panel of representative protein bands. (C) Protein levels of PI3K [PI3-kinase p85α (54 + 85 kDa)], phosphorylated-AKT and FoxO1 in kidney tissues (n=6). Corresponding histograms are shown on the right panel of representative protein bands. *P<0.05, **P<0.01 and ***P<0.001. p-, phosphorylated.

controls (Fig. 7C). Both HG exposure and C3aR knockdown similarly activated PI3K/AKT signaling and reduced FoxO1, while C3aR inhibition reversed these effects (Fig. 7D), consistent with the aforementioned *in vivo* data. Under HG conditions with C3a overexpression, treatment with LY294002 (a PI3K inhibitor; cat. no. HY-10108; MedChemExpress), which was dissolved in DMSO and applied to podocytes at a final concentration of 20 μM for 24 h prior to protein extraction, reduced PI3K/AKT phosphorylation, restored FoxO1 expression and increased the number of mitochondrial $LC3^{+}$ puncta (by 2.3-fold, P<0.001) with elevated mitophagic flux (Fig. 7E and F). C3a induced FoxO1 nuclear export through enhanced phosphorylation, a process that was significantly attenuated by LY294002 (Fig. 7G). These results indicated that C3a/C3aR mediates hyperglycemia-induced podocytopathy by suppressing mitophagy through PI3K/AKT-dependent inhibition of FoxO1-PINK1 signaling.

Discussion

Increasing evidence suggests that the complement system and its downstream components contribute to the development of DN (19). The kidneys, in a diabetic state, are continuously exposed to metabolic and hemodynamic stress, leading to cellular damage and activation of innate immune responses, including the complement system (20), with complement C3 serving as the central hub in the complement cascade (21). Previous studies have indicated that patients and animals with DN exhibit renal glomerular C3 deposition (4,22). In the present study, a markedly higher expression of C3 and C3aR was observed in podocytes of patients with DN compared with those of patients with other kidney-related diseases. This suggests that complement system activation, particularly the C3a/C3aR axis, is closely associated with HG-induced kidney damage and proteinuria. Based on clinical problems,

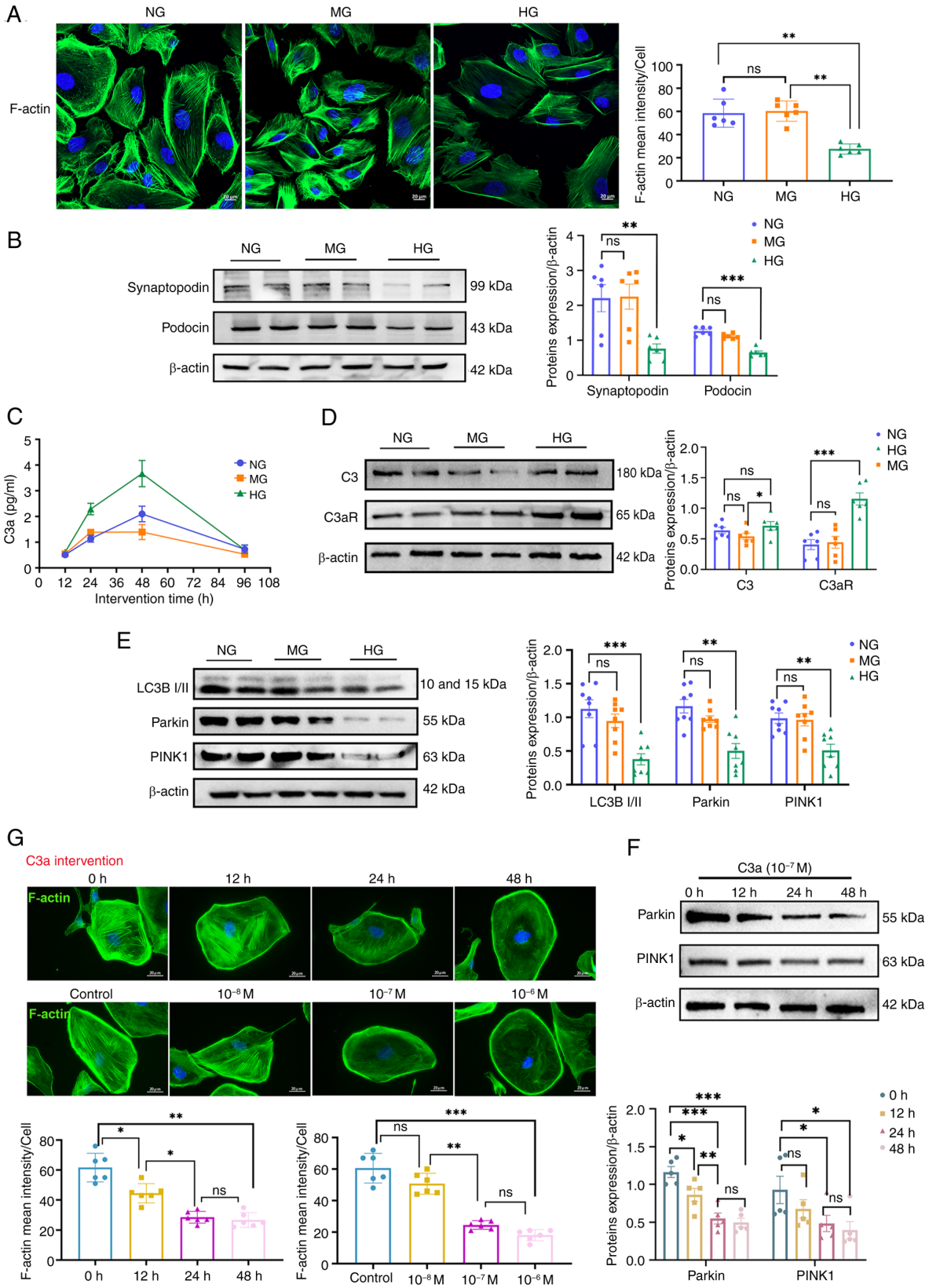

Figure 5. Effects of HG and C3a on podocyte damage and mitophagy. Normal glucose refers to 5.5 mM glucose, while the mannitol high osmotic control group was subjected to 24.5 mM mannitol + 5.5 mM glucose, and HG represents the intervention group (30 mM glucose). (A) Representative images (left) and quantification (right) of podocyte cytoskeleton, with F-actin (green) stained using phalloidin (n=6). Scale bar, 20 μm. (B) Protein levels of synaptopodin and podocin in podocytes (n=6). Corresponding histograms are shown on the bottom panel of representative protein bands. (C) ELISA detection of C3a levels in podocytes at different time points (n=6). (D) Protein levels of C3 and C3aR in podocytes (n=6). Corresponding histograms are shown on the right panel of representative protein bands. (E) Protein levels of LC3B I/II, parkin and PINK1 in podocytes (n=8). Corresponding histograms are shown on the bottom panel of representative protein bands. (F) Protein levels of parkin and PINK1 in podocytes (n=5). Corresponding histograms are shown on the right panel of representative protein bands. (G) Representative images and quantification (bottom) of podocyte cytoskeleton induced by different times and concentrations of C3a (10^{-7} M for 12, 24 and 48 h; or 10^{-8}, 10^{-7} and 10^{-6} M for 24 h) (n=6). Scale bar, 20 μm. *P<0.05, **P<0.01 and ***P<0.001. ns, no statistically significant difference; HG, high glucose.

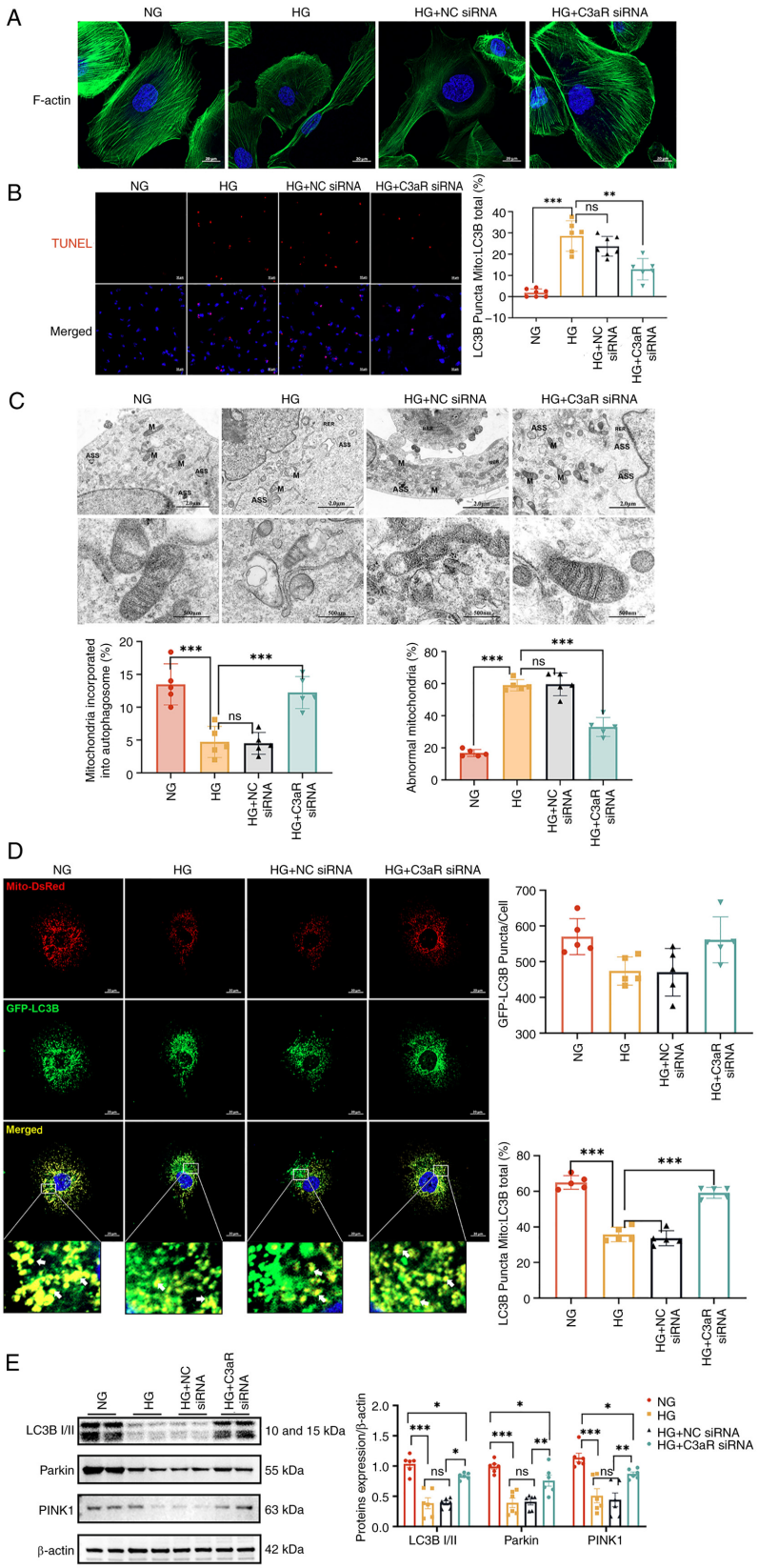

Figure 6. Inhibition of C3aR improves HG-induced podocyte and mitochondrial autophagic damage. (A) Changes in cell cytoskeleton after blocking C3aR in a HG environment. Scale bar, 20 μm. (B) Immunofluorescence images of podocytes in each group using a TdT-mediated dUTP nick-end labeling assay. Scale bar, 50 μm. The lower panel presents the statistical analysis of apoptosis ratios in podocytes for each group (n=6). (C) Transmission electron microscopy examination of mitochondrial morphology. Scale bar, 2.0 μm and 500 nm. The statistical charts on the right side of the electron microscopy images represent the percentages of damaged mitochondria and mitochondria enveloped by autophagosomes (n=5). (D) Transfection of immortalized human podocytes with adenovirus GFP-LC3B (green) and DsRed-Mito (red). Scale bar, 20 μm. The statistical charts on the right side represent the number of GFP-LC3B-positive puncta per cell and the proportion of LC3B spots on mitochondria (Mito) to total LC3B. Quantification of GFP-LC3B (green)-associated Mito-DsRed (red) staining intensity normalized by GFP-LC3B area (n=5). (E) Protein levels of LC3B I/II, parkin and PINK1 in podocytes (n=6). Corresponding histograms are shown on the right panel of representative protein bands. *P<0.05, **P<0.01 and ***P<0.001. ns, no statistically significant difference; HG, high glucose; NG, normal glucose; siRNA, small interfering RNA; NC, negative control.

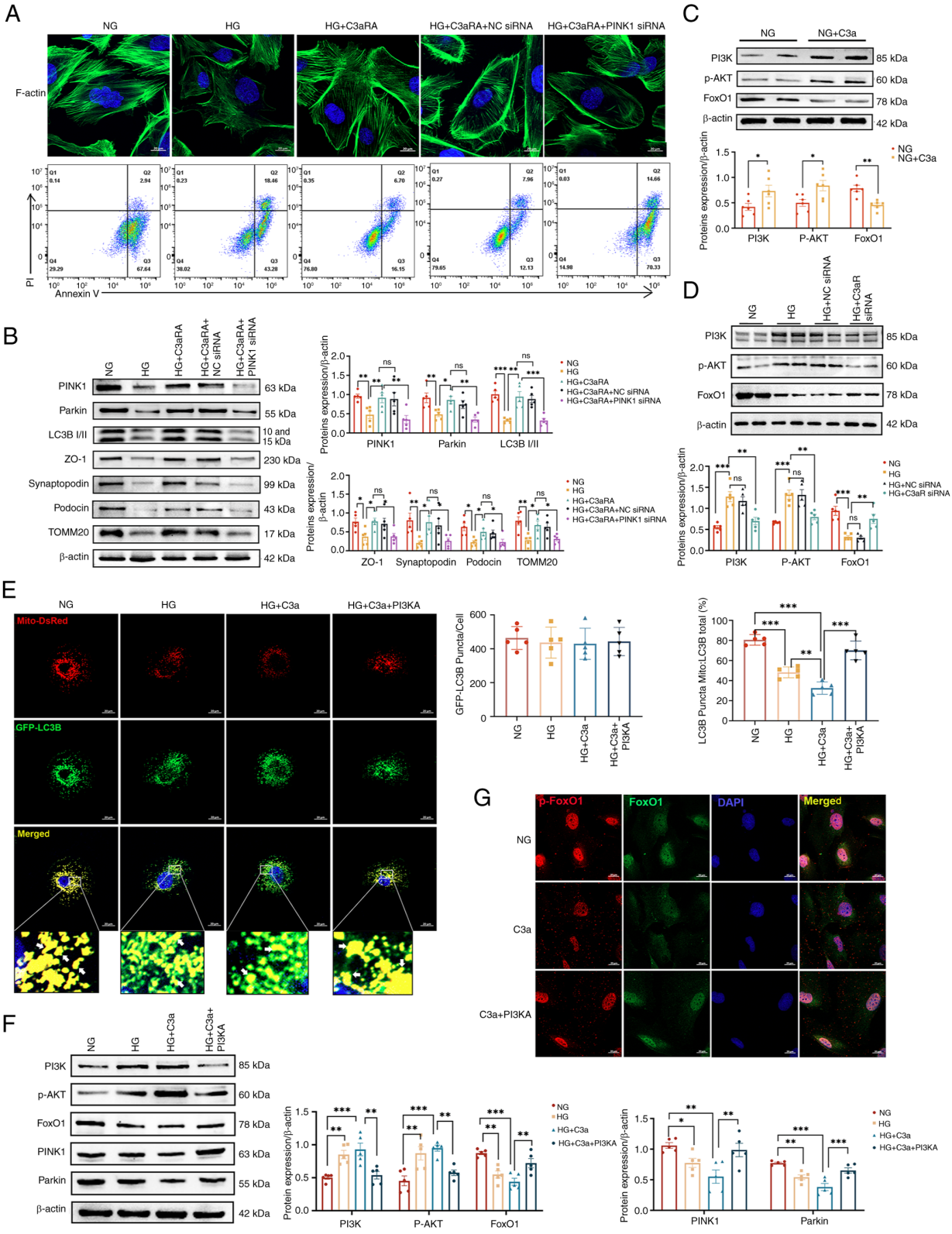

Figure 7. C3a downregulates mitophagy levels through the PI3K/AKT/FoxO1 signaling pathway in a HG environment, leading to podocyte damage. (A) Immunofluorescence images of F-actin-stained podocyte cytoskeleton. Scale bar, 20 μm. Flow cytometric analysis of podocyte apoptosis under different intervention conditions using annexin V-FITC PI. (B) Expression of podocyte functional and mitophagy-related proteins after PINK1 inhibition (n=5). Corresponding histograms are shown on the right panel of representative protein bands. (C) Expression of downstream signaling molecules after direct stimulation of podocytes by C3a (n=6). (D) Expression of downstream signaling molecules after inhibiting C3aR in a HG environment (n=5). Corresponding histograms are shown on the bottom panel of the representative protein bands. (E) Confocal microscopy images capturing fluorescence of immortalized human podocytes transfected with adenovirus GFP-LC3B (green) and Mito-DsRed (red). Scale bar, 20 μm. The right panel represents the statistical analysis of the number of GFP-LC3B-positive spots per cell and the proportion of LC3B spots on mitochondria (Mito) to total LC3B. Quantification of GFP-LC3B-associated Mito-DsRed staining intensity normalized by GFP-LC3B area (n=5). (F) Effects of PI3K inhibition on downstream pathway proteins and mitophagy proteins under HG conditions with *C3a* overexpression (n=5). Corresponding histograms are shown on the bottom panel of representative protein bands. (G) Immunofluorescence micrographs demonstrating the nuclear/cytoplasmic distribution of FoxO1 in podocytes, with dual-color staining of phosphoryalted-FoxO1 (red) and FoxO1 (green). Scale bar, 20 μm. *P<0.05, **P<0.01 and ***P<0.001. ns, no statistically significant difference; HG, high-glucose.

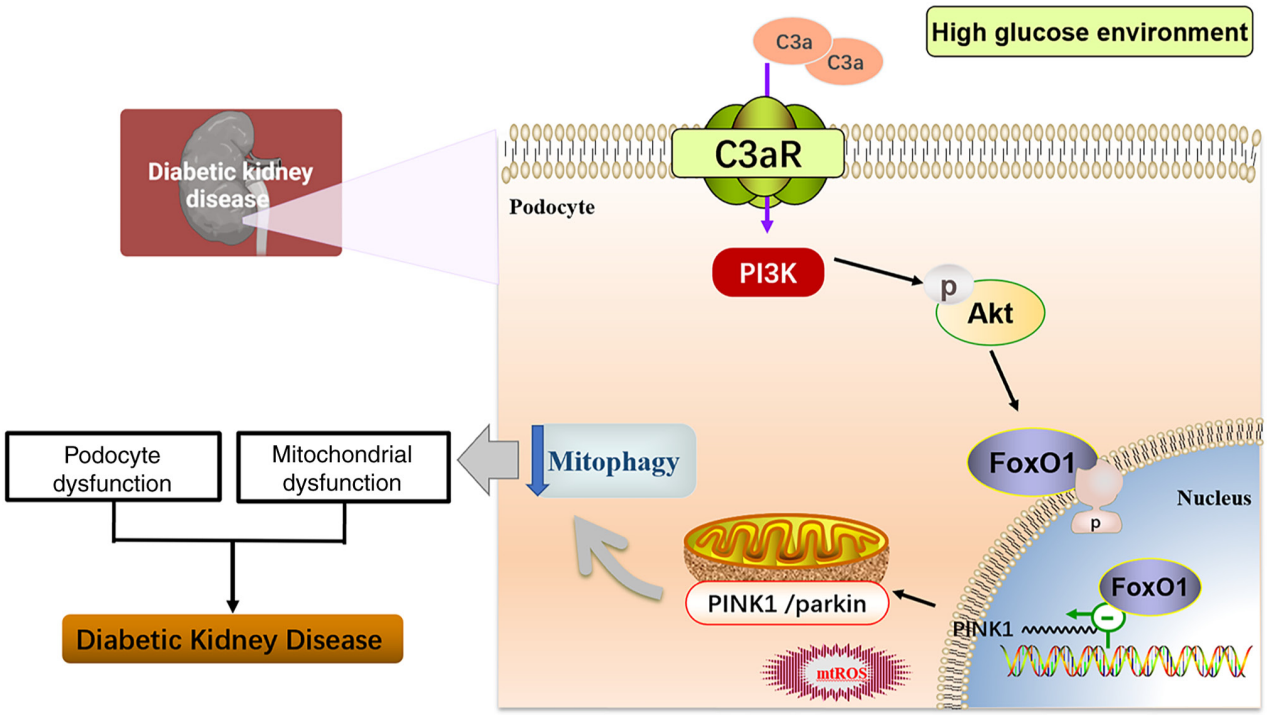

Figure 8. Role and mechanism of C3a/C3aR in a DN model. In a high-glucose environment, the complement component C3 is activated. The C3a/C3aR axis modulates the PI3K-AKT signaling pathway, resulting in an enhanced phosphorylation level of FoxO1, leading to the loss of its transcriptional activity. Consequently, there is inhibition of PINK1/parkin-mediated mitophagy, contributing to podocyte injury and DN progression. DN, diabetic nephropathy; C3aRA, C3aR antagonist.

db/db mice were employed to simulate the process of renal damage in clinical DN, which is a spontaneous diabetic mouse model with leptin receptor gene deficiency. Compared with the STZ-induced type 2 diabetes mouse model, db/db mice showed obesity and more obvious renal damage. In addition, the occurrence of diabetes in db/db mice is more similar to that in clinical patients with type 2 diabetes because there is no artificial interference (23,24).

In the current study, db/db mice exhibited C3 deposition and elevated C3aR levels, accompanied with podocyte loss, increased levels of proteinuria and renal tissue damage. Podocyte apoptosis can result in podocyte loss and damage, exacerbating the severity of proteinuria in patients with DN (25,26). Previous literature has reported that the C3a/C3aR axis in podocytes can initiate autocrine IL-1β/IL-1R1 signaling, downregulating nephrin expression and leading to rearrangement of the actin cytoskeleton (27). Similarly, in the present study, blocking C3aR increased the expression of the podocyte functional proteins nephrin and synaptopodin in DN mice glomeruli, and improved podocyte cytoskeleton alignmen in HG. This suggests the involvement of the C3a/C3aR axis in podocyte damage in DN, which is primarily manifested in cytoskeleton disruption and downregulation of nephrin expression, with C3aRAs potentially contributing to the maintenance of podocyte homeostasis.

Podocytes exhibit high dynamism, thus necessitating substantial energy to maintain the normal organization of the cytoskeleton and podocyte foot process remodeling (28). Impaired mitophagy is considered a hallmark of human DN and rodent models of DN (29). Currently, the PINK1/parkin pathway is considered one of the most crucial mediators in the process of mitophagy (30). The present study confirmed a decrease in PINK1/parkin-mediated mitophagy levels in the db/db mice and in podocytes under HG conditions *in vitro*. Similarly, reduced PINK1/parkin mitophagy has been reported in HK-2 cells under HG conditions, STZ-induced DN models (12,31), proximal tubular cells (32), glomerular mesangial cells (33), podocytes, and db/db mouse models of DN (34), aligning with the current findings. By contrast, certain previous studies have reported abnormal activation of PINK1/parkin-mediated mitophagy in db/db mice (35,36). The db/db mice model effectively recapitulates early-stage DN manifestations, including characteristic glomerular pathology, podocyte injury and the albuminuric phase, but fails to develop progressive renal fibrosis or end-stage renal disease (ESRD) features typically observed in advanced human DN, primarily due to its constrained 24-week observation window, species-specific attenuation of fibrotic pathways, and absence of sustained glomerulosclerosis that would culminate in functional renal failure, thereby limiting its translational relevance for late-stage DN therapeutic interventions requiring fibrosis or ESRD endpoints. The db/db mice model remains the gold standard for initiating events in DN but necessitates complementary approaches for disease culmination studies. In subsequent studies, therapeutic strategies targeting fibrosis/ESRD reversal must be validated using complementary models (for example, uninephrectomized db/db mice or DBA/2J-STZ mice). These seemingly disparate results may be attributed to different stages of DN. In the early stages of DN, the number of damaged mitochondria increases, and compensatory mitophagy is enhanced to eliminate these mitochondria. As DN progresses to a certain stage, compensatory mitophagy

becomes insufficient to clear an adequate number of damaged mitochondria, resulting in a decompensated state and a decrease in mitophagy levels (37). Since there were no genetic background differences in the animals used in these studies, further research is needed to explain these conflicting results observed in the activation pattern of PINK1/parkin-mediated mitophagy.

Numerous previous studies, including one conducted by our group, have reported the key role of C3a/C3aR in accelerating apoptosis. CRP interacts with the C3a/C3aR axis to promote the process of DN through podocyte autophagy (38), and the treatment of DN mice with a C3aRA enhanced podocyte density and preserved their phenotype, limiting proteinuria and glomerular injury (8). Overall, this suggests that the C3a/C3aR axis plays an important role in diabetic podocyte injury, which may involve podocyte autophagy. The current study also found that C3aR blockade protected podocytes and mitochondria from damage in DN, as evidence by the corresponding changes in mitophagy levels during the process. The majority of previous studies have shown significant changes in the expression of mitophagy-related genes in the entire lysates of kidney tissues or cells, with little localization within mitochondria. Although the C3a/C3aR axis has been demonstrated to affect mitochondrial biogenesis, including impairing PPARα/CPT-1α-mediated renal tubular mitochondrial fatty acid oxidation (39), there is currently no relevant research on the involvement of the C3a/C3aR axis in podocyte mitophagy. In the present study, Mito-LC3B adenovirus was utilized for exogenous transfection of immortalized human podocytes, and the co-localization assessment of mitochondria and lysosomes helped further elucidate the role of PINK1/parkin-mediated mitophagy in C3a-induced podocyte damage under HG conditions. The results revealed a significant decrease in mitophagy flux in podocytes cultured in a HG environment compared with the NG control group. Inhibition of C3aR improved the reduced mitophagy induced by HG, confirming that the C3a/C3aR axis downregulates mitophagy levels in podocytes, participating in the process of podocyte damage. While initially characterized as a C3aR antagonist, subsequent studies have demonstrated that SB290157 inhibits C5aR1 (Ki≈1 μM) at higher concentrations, and C5aR1 similarly mediates inflammation and podocyte injury in DN. Moreover, SB290157 exhibits concentration-dependent (>μM) activation of PAR1 and PAR2, both expressed in renal cells. To mitigate these potential off-target effects, our experimental design rigorously maintained concentrations ≤0.5 μM. Furthermore, complementary C3aR siRNA experiments in cellular models confirmed that the pharmacological profile of SB290157 persisted under these constrained conditions.

The present study delineates a novel mechanistic link between the C3a/C3aR axis and podocyte mitophagy dysregulation in DN, centrally orchestrated by the PI3K/AKT/FoxO1 signaling pathway. Numerous previous studies have reported the activation of the PI3K/AKT pathway in DN animal models (40-43), and that inhibiting the PI3K/AKT pathway could enhance podocyte autophagy levels and reduce proteinuria (44,45). In the present study, increased expression of PI3K/AKT signaling molecules was observed in the renal tissues of db/db mice and in podocytes cultured in a HG environment *in vitro*. Blocking C3aR expression inhibited the PI3K/AKT signaling pathway. Inhibition of PI3K/AKT signaling prevents phosphorylation of FoxO1, enabling its nuclear translocation, thereby regulating gene expression associated with cell death, proliferation, differentiation, cellular metabolism, and oxidative stress (46,47). Previous studies have established that PI3K/AKT signaling exacerbates insulin resistance in diabetes by inhibiting FOXO-driven metabolic adaptations (48,49). FoxO1 overexpression prevents podocyte damage and improves the progression of DN (50). The current study uncovers that C3a, a complement effector, acts as an upstream trigger of PI3K/AKT in podocytes. In diabetic environments, C3aR binding activates PI3K/AKT, which subsequently phosphorylates and inactivates FoxO1. This redirects FoxO1 from the nucleus to the cytoplasm, repressing the transcription of mitophagy genes (such as PINK1 and parkin). The current findings support the observations that C3aR blockade restores mitochondrial integrity, mechanistically linking complement to FoxO1-driven redox and metabolic homeostasis. However, in the present study, only PI3K inhibitors were used, and the expression changes of the downstream signal molecules AKT and FoxO1 were indirectly detected. Their direct role and existence in the nucleus or cytoplasm are not yet clear; thus, further studies are required in the future.

Additionally, a limitation of the present study is that the exclusive focus on complement C3 and C3aR, lacking the assessment of complement fragment C3a levels. Although a significant increase in C3a under HG conditions was detected *in vitro* in cultured podocytes, no noticeable differences in circulating C3a expression were observed in the mouse experiments. Considering the possibility of localized activation of complement C3a in the kidney, future studies should construct models to measure C3a levels in urine or locally collected blood from the kidneys.

In summary (Fig. 8), the present study demonstrated for the first time that the C3a/C3aR axis regulates the PI3K/AKT/FoxO1 signaling pathway, and then leads to diabetic renal injury by inhibiting podocyte mitophagy, suggesting that blocking C3aR may be an innovative therapeutic strategy for treating patients with DN.

Acknowledgements

The authors acknowledge Professor Liangdi Xie from the Fujian Hypertension Research Institute, The First Affiliated Hospital of Fujian Medical University for his providing the experimental site and instruments. Additionally, the authors would like to thank Mr Changshen Xu and Ms Guili Lian from the Fujian Hypertension Research Institute, The First Affiliated Hospital of Fujian Medical University for their technical assistance and research resources. The authors also thank the Public Technology Platform, The First Affiliated Hospital of Fujian Medical University for its technical support.

Funding

The present study was supported by the Fujian Provincial Health Technology Project (grant no. 2021CXA018), the National Natural Science Foundation of China (grant nos. 82470733 and 82401848).

Availability of data and materials

The data generated in the present study may be requested from the corresponding author.

Authors' contributions

MW and JW conceived and designed the study. MW, XW, SR, TZ and JZ performed the experiments. JC, XW, SR, EL, DY and KN analyzed the data. MW was a major contributor in writing the manuscript. JW and MW assume overall responsibility for the manuscript. JW and JC confirm the authenticity of all the raw data. JW and JC was responsible for supervision, funding acquisition and interpretation of data. All authors read and approved the final version of the manuscript.

Ethics approval and consent to participate

All procedures were conducted in accordance with the NIH Guide for the Care and Use of Laboratory Animals and approved by the Institutional Animal Care and Use Committee of Fujian Medical University (approval no. IACUC FJMU 2023-Y-1033; Fuzhou, China).

Patient consent for publication

Not applicable.

Competing interests

The authors declare that they have no competing interests.

References

1. Ma J, Yiu WH and Tang SCW: Complement anaphylatoxins: Potential therapeutic target for diabetic kidney disease. Diabet Med 42: e15427, 2025.
2. Li X, Zhao S, Xie J, Li M, Tong S, Ma J, Yang R, Zhao Q, Zhang J and Xu A: Targeting the NF-κB p65-MMP28 axis: Wogonoside as a novel therapeutic agent for attenuating podocyte injury in diabetic nephropathy. Phytomedicine 138: 156406, 2025.
3. Wang T, Chen Y, Liu Z, Zhou J, Li N, Shan Y and He Y: Long noncoding RNA Glis2 regulates podocyte mitochondrial dysfunction and apoptosis in diabetic nephropathy via sponging miR-328-5p. J Cell Mol Med 28: e18204, 2024.
4. Woroniecka KI, Park ASD, Mohtat D, Thomas DB, Pullman JM and Susztak K: Transcriptome analysis of human diabetic kidney disease. Diabetes 60: 2354-2369, 2011.
5. Wehner H, Höhn D, Faix-Schade U, Huber H and Walzer P: Glomerular changes in mice with spontaneous hereditary diabetes. Lab Invest 27: 331-340, 1972.
6. Li L, Chen L, Zang J, Tang X, Liu Y, Zhang J, Bai L, Yin Q, Lu Y, Cheng J, *et al*: C3a and C5a receptor antagonists ameliorate endothelial-myofibroblast transition via the Wnt/β-catenin signaling pathway in diabetic kidney disease. Metabolism 64: 597-610, 2015.
7. Li L, Yin Q, Tang X, Bai L, Zhang J, Gou S, Zhu H, Cheng J, Fu P and Liu F: C3a receptor antagonist ameliorates inflammatory and fibrotic signals in type 2 diabetic nephropathy by suppressing the activation of TGF-β/smad3 and IKBα pathway. PLoS One 9: e113639, 2014.
8. Morigi M, Perico L, Corna D, Locatelli M, Cassis P, Carminati CE, Bolognini S, Zoja C, Remuzzi G, Benigni A and Buelli S: C3a receptor blockade protects podocytes from injury in diabetic nephropathy. JCI Insight 5: e131849, 2020.
9. Ma K, Chen G, Li W, Kepp O, Zhu Y and Chen Q: Mitophagy, mitochondrial homeostasis, and cell fate. Front Cell Dev Biol 8: 467, 2020.
10. Stanigut AM, Tuta L, Pana C, Alexandrescu L, Suceveanu A, Blebea NM and Vacaroiu IA: Autophagy and mitophagy in diabetic kidney disease-a literature review. Int J Mol Sci 26: 806, 2025.
11. Tagawa A, Yasuda M, Kume S, Yamahara K, Nakazawa J, Chin-Kanasaki M, Araki H, Araki S, Koya D, Asanuma K, *et al*: Impaired podocyte autophagy exacerbates proteinuria in diabetic nephropathy. Diabetes 65: 755-767, 2016.
12. Zhou D, Zhou M, Wang Z, Fu Y, Jia M, Wang X, Liu M, Zhang Y, Sun Y, Zhou Y, *et al*: Progranulin alleviates podocyte injury via regulating CAMKK/AMPK-mediated autophagy under diabetic conditions. J Mol Med (Berl) 97: 1507-1520, 2019.
13. Zhou D, Zhou M, Wang Z, Fu Y, Jia M, Wang X, Liu M, Zhang Y, Sun Y, Lu Y, *et al*: PGRN acts as a novel regulator of mitochondrial homeostasis by facilitating mitophagy and mitochondrial biogenesis to prevent podocyte injury in diabetic nephropathy. Cell Death Dis 10: 524, 2019.
14. Martini S, Nair V, Keller BJ, Eichinger F, Hawkins JJ, Randolph A, Böger CA, Gadegbeku CA, Fox CS, Cohen CD, *et al*: Integrative biology identifies shared transcriptional networks in CKD. J Am Soc Nephrol 25: 2559-2572, 2014.
15. Ju W, Greene CS, Eichinger F, Nair V, Hodgin JB, Bitzer M, Lee YS, Zhu Q, Kehata M, Li M, *et al*: Defining cell-type specificity at the transcriptional level in human disease. Genome Res 23: 1862-1873, 2013.
16. National Research Council Committee for the Update of the Guide for the, C. and A. Use of Laboratory. The National Academies Collection: Reports funded by National Institutes of Health, in Guide for the Care and Use of Laboratory Animals. National Academies Press. Copyright© 2011. National Academy of Sciences, Washington, DC, 2011.
17. Ames RS, Lee D, Foley JJ, Jurewicz AJ, Tornetta MA, Bautsch W, Settmacher B, Klos A, Erhard KF, Cousins RD, *et al*: Identification of a selective nonpeptide antagonist of the anaphylatoxin C3a receptor that demonstrates antiinflammatory activity in animal models. J Immunol 166: 6341-6348, 2001.
18. Yasuda-Yamahara M, Kume S, Tagawa A, Maegawa H and Uzu T: Emerging role of podocyte autophagy in the progression of diabetic nephropathy. Autophagy 11: 2385-2386, 2015.
19. Flyvbjerg A: The role of the complement system in diabetic nephropathy. Nat Rev Nephrol 13: 311-318, 2017.
20. Tesch GH: Diabetic nephropathy-is this an immune disorder? Clin Sci (Lond) 131: 2183-2199, 2017.
21. Sahu A and Lambris JD: Structure and biology of complement protein C3, a connecting link between innate and acquired immunity. Immunol Rev 180: 35-48, 2001.
22. Kelly KJ, Liu Y, Zhang J and Dominguez JH: Renal C3 complement component: Feed forward to diabetic kidney disease. Am J Nephrol 41: 48-56, 2015.
23. Racine KC, Iglesias-Carres L, Herring JA, Wieland KL, Ellsworth PN, Tessem JS, Ferruzzi MG, Kay CD and Neilson AP: The high-fat diet and low-dose streptozotocin type-2 diabetes model induces hyperinsulinemia and insulin resistance in male but not female C57BL/6J mice. Nutr Res 131: 135-146, 2024.
24. Wang L, Zhou R, Li G, Zhang X, Li Y, Shen Y and Fang J: Multi-omics characterization of diabetic nephropathy in the db/db mouse model of type 2 diabetes. Comput Struct Biotechnol J 27: 3399-3409, 2025.
25. Jin J, Shi Y, Gong J, Zhao L, Li Y, He Q and Huang H: Exosome secreted from adipose-derived stem cells attenuates diabetic nephropathy by promoting autophagy flux and inhibiting apoptosis in podocyte. Stem Cell Res Ther 10: 95, 2019.
26. Yuen DA, Stead BE, Zhang Y, White KE, Kabir MG, Thai K, Advani SL, Connelly KA, Takano T, Zhu L, *et al*: eNOS deficiency predisposes podocytes to injury in diabetes. J Am Soc Nephrol 23: 1810-1823, 2012.
27. Angeletti A, Cantarelli C, Petrosyan A, Andrighetto S, Budge K, D'Agati VD, Hartzell S, Malvi D, Donadei C, Thurman JM, *et al*: Loss of decay-accelerating factor triggers podocyte injury and glomerulosclerosis. J Exp Med 217: e20191699, 2020.
28. Galvan DL, Green NH and Danesh FR: The hallmarks of mitochondrial dysfunction in chronic kidney disease. Kidney Int 92: 1051-1057, 2017.
29. Chen K, Dai H, Yuan J, Chen J, Lin L, Zhang W, Wang L, Zhang J, Li K and He Y: Optineurin-mediated mitophagy protects renal tubular epithelial cells against accelerated senescence in diabetic nephropathy. Cell Death Dis 9: 105, 2018.
30. Nguyen TN, Padman BS and Lazarou M: Deciphering the molecular signals of PINK1/parkin mitophagy. Trends Cell Biol 26: 733-744, 2016.

31. Li W, Du M, Wang Q, Ma X, Wu L, Guo F, Ji H, Huang F and Qin G: FoxO1 promotes mitophagy in the podocytes of diabetic male mice via the PINK1/parkin pathway. Endocrinology 158: 2155-2167, 2017.
32. Zhao Y and Sun M: Metformin rescues Parkin protein expression and mitophagy in high glucose-challenged human renal epithelial cells by inhibiting NF-κB via PP2A activation. Life Sci 246: 117382, 2020.
33. Yi X, Yan W, Guo T, Liu N, Wang Z, Shang J, Wei X, Cui X, Sun Y, Ren S and Chen L: Erythropoietin mitigates diabetic nephropathy by restoring PINK1/Parkin-mediated mitophagy. Front Pharmacol 13: 883057, 2022.
34. Sun J, Zhu H, Wang X, Gao Q, Li Z and Huang H: CoQ10 ameliorates mitochondrial dysfunction in diabetic nephropathy through mitophagy. J Endocrinol 240: 445-465, 2019.
35. Liu X, Wang W, Song G, Wei X, Zeng Y, Han P, Wang D, Shao M, Wu J, Sun H, *et al*: Astragaloside IV ameliorates diabetic nephropathy by modulating the mitochondrial quality control network. PLoS One 12: e0182558, 2017.
36. Liu X, Lu J, Liu S, Huang D, Chen M, Xiong G and Li S: Huangqi-Danshen decoction alleviates diabetic nephropathy in db/db mice by inhibiting PINK1/Parkin-mediated mitophagy. Am J Transl Res 12: 989-998, 2020.
37. Yang M, Li C, Yang S, Xiao Y, Chen W, Gao P, Jiang N, Xiong S, Wei L, Zhang Q, *et al*: Mitophagy: A novel therapeutic target for treating DN. Curr Med Chem 28: 2717-2728, 2021.
38. Zhang L, Li W, Gong M, Zhang Z, Xue X, Mao J, Zhang H, Li S, Liu X, Wu F, *et al*: C-reactive protein inhibits C3a/C3aR-dependent podocyte autophagy in favor of diabetic kidney disease. FASEB J 36: e22332, 2022.
39. Wang C, Wang Z, Xu J, Ma H, Jin K, Xu T, Pan X, Feng X and Zhang W: C3aR antagonist alleviates C3a induced tubular profibrotic phenotype transition via restoring PPARα/CPT-1α mediated mitochondrial fatty acid oxidation in renin-dependent hypertension. Front Biosci (Landmark Ed) 28: 238, 2023.
40. Chen Y, Zheng YF, Lin XH, Zhang JP, Lin F and Shi H: Dendrobium mixture attenuates renal damage in rats with diabetic nephropathy by inhibiting the PI3K/Akt/mTOR pathway. Mol Med Rep 24: 590, 2021.
41. Ma Z, Liu Y, Li C, Zhang Y and Lin N: Repurposing a clinically approved prescription Colquhounia root tablet to treat diabetic kidney disease via suppressing PI3K/AKT/NF-kB activation. Chin Med 17: 2, 2022.
42. Dong R, Zhang X, Liu Y, Zhao T, Sun Z, Liu P, Xiang Q, Xiong J, Du X, Yang X, *et al*: Rutin alleviates EndMT by restoring autophagy through inhibiting HDAC1 via PI3K/AKT/mTOR pathway in diabetic kidney disease. Phytomedicine 112: 154700, 2023.
43. Zhang Y, Yang S, Cui X, Yang J, Zheng M, Jia J, Han F, Yang X, Wang J, Guo Z, *et al*: Hyperinsulinemia can cause kidney disease in the IGT stage of OLETF rats via the INS/IRS-1/PI3-K/Akt signaling pathway. J Diabetes Res 2019: 4709715, 2019.
44. Zheng D, Tao M, Liang X, Li Y, Jin J and He Q: p66Shc regulates podocyte autophagy in high glucose environment through the Notch-PTEN-PI3K/Akt/mTOR pathway. Histol Histopathol 35: 405-415, 2020.
45. Wang X, Jiang L, Liu XQ, Huang YB, Wang AL, Zeng HX, Gao L, Zhu QJ, Xia LL and Wu YG: Paeoniflorin binds to VEGFR2 to restore autophagy and inhibit apoptosis for podocyte protection in diabetic kidney disease through PI3K-AKT signaling pathway. Phytomedicine 106: 154400, 2022.
46. Chen Y, Li Z, Li H, Su W, Xie Y, Pan Y, Chen X and Liang D: Apremilast regulates the Teff/Treg balance to ameliorate uveitis via PI3K/AKT/FoxO1 signaling pathway. Front Immunol 11: 581673, 2020.
47. Miao Z, Liu Y, Xu Y, Bu J and Yang Q: Oxaloacetate promotes the transition from glycolysis to gluconeogenesis through the Akt-FoxO1 and JNK/c-Jun-FoxO1 axes and inhibits the survival of liver cancer cells. Int Immunopharmacol 161: 115051, 2025.
48. Xu Z, Liu K, Zhang G, Yang F, He Y, Nan W, Li Y and Lin J: Transcriptome analysis reveals that the injection of mesenchymal stem cells remodels extracellular matrix and complement components of the brain through PI3K/AKT/FOXO1 signaling pathway in a neuroinflammation mouse model. Genomics 117: 111033, 2025.
49. Deng A, Wang Y, Huang K, Xie P, Mo P, Liu F, Chen J, Chen K, Wang Y and Xiao B: Artichoke (Cynara scolymus L.) water extract alleviates palmitate-induced insulin resistance in HepG2 hepatocytes via the activation of IRS1/PI3K/AKT/FoxO1 and GSK-3β signaling pathway. BMC Complement Med Ther 23: 460, 2023.
50. Cosenso-Martin LN, Takaoka LY and Vilela-Martin JF: Randomized study comparing vildagliptin vs glibenclamide on glucose variability and endothelial function in patients with type 2 diabetes mellitus and hypertension. Diabetes Metab Syndr Obes 13: 3221-3229, 2020.